LU TP 00–10
LBNL-45275
hep-ph/0003056
March 2000

Bottom Production Asymmetries at the LHC[1]

E. Norrbin[2]

Department of Theoretical Physics,
Lund University, Lund, Sweden

and

R. Vogt[3]

Physics Department,
University of California at Davis
and
Nuclear Science Division,
Lawrence Berkeley National Laboratory

Abstract

We present results on bottom hadron production asymmetries at the LHC within both the Lund string fragmentation model and the intrinsic bottom model. The main aspects of the models are summarized and specific predictions for pp collisions at 14 TeV are given. Asymmetries are found to be very small at central rapidities increasing to a few percent at forward rapidities. At very large rapidities intrinsic production could dominate but this region is probably out of reach of any experiment.

[1]To appear in the proceedings of the "CERN 1999 Workshop on SM physics (and more) at the LHC".

[2]emanuel@thep.lu.se
[3]vogt@lbl.gov

[3]This work was supported in part by the Director, Office of Energy Research, Division of Nuclear Physics of the Office of High Energy and Nuclear Physics of the U. S. Department of Energy under Contract Number DE-AC03-76SF00098.

1 Introduction

Sizeable leading particle asymmetries between e.g. D^- and D^+ have been observed in several fixed target experiments [1]. It is of interest to investigate to what extent these phenomena translate to bottom production and higher energies. No previous experiment has observed asymmetries for bottom hadrons due to limited statistics or other experimental obstacles. Bottom asymmetries are in general expected to be smaller than for charm because of the larger bottom mass, but there is no reason why they should be absent. In the fixed target experiment HERA-B, bottom asymmetries could very well be large [2] even at central rapidities, but the conclusion of the present study is that asymmetries at the LHC are likely to be small. In the following we study possible asymmetries between B and $\overline{\mathrm{B}}$ hadrons at the LHC within the Lund string fragmentation model [3] and the intrinsic heavy quark model [4].

In the string fragmentation model [5], the perturbatively produced heavy quarks are colour connected to the beam remnants. This gives rise to beam-drag effects where the heavy hadron can be produced at larger rapidities than the heavy quark. The extreme case in this direction is the collapse of a small string, containing a heavy quark and a light beam remnant valence quark of the proton, into a single hadron. This gives rise to flavour correlations which are observed as asymmetries. Thus, in the string model, there can be coalescence between a perturbatively produced bottom quark and a light quark in the beam remnant producing a leading bottom hadron.

There is also the possibility to have coalescence between the light valence quarks and bottom quarks already present in the proton, because the wavefunction of the proton can fluctuate into Fock configurations containing a $\mathrm{b\overline{b}}$ pair, such as $|\mathrm{uudb\overline{b}}\rangle$. In these states, two or more gluons are attached to the bottom quarks, reducing the amplitude by $\mathcal{O}(\alpha_s^2)$ relative to parton fusion [6]. The longest-lived fluctuations in states with invariant mass M have a lifetime of $\mathcal{O}(2P_{\mathrm{lab}}/M^2)$ in the target rest frame, where P_{lab} is the projectile momenta. Since the comoving bottom and valence quarks have the same rapidity in these states, the heavy quarks carry a large fraction of the projectile momentum and can thus readily combine to produce bottom hadrons with large longitudinal momenta. Such a mechanism can then dominate the hadroproduction rate at large x_{F}. This is the underlying assumption of the intrinsic heavy quark model [4], in which the wave function fluctuations are initially far off shell. However, they materialize as heavy hadrons when light spectator quarks in the projectile Fock state interact with the target [7].

In both models the coalescence probability is largest at small relative rapidity and rather low transverse momentum where the invariant mass of the $\overline{\mathrm{Q}}\mathrm{q}$ system is small, enhancing the binding amplitude. One exception is at very large $p_\perp$, where the collapse of a scattered valence quark with a $\overline{\mathrm{b}}$ quark from the parton shower is also possible, giving a further (small) source of leading particle asymmetries in the string model.

2 Lund String Fragmentation

Before describing the Lund string fragmentation model, some words on the perturbative heavy quark production mechanisms included in the Monte Carlo event generator Pythia [8] used in this study is in order. We study pp events with one hard interaction because events with no hard interaction are not expected to produce heavy flavours and events with more than one hard interaction — multiple interactions — are beyond the scope of this initial study and presumably would not influence the asymmetries. After the hard interaction is generated, parton showers are added, both to the initial (ISR) and final (FSR) state. The branchings in the shower are taken to be of lower virtualities than the hard interaction introducing a virtuality (or time) ordering in the event. This approach gives rise to several heavy quark production mechanisms, which we will call *pair creation*, *flavour excitation* and *gluon splitting*. The names may be somewhat misleading since all three classes create pairs at $\mathrm{g} \to \mathrm{Q}\overline{\mathrm{Q}}$ vertices, but it is in line with the colloquial nomenclature. The three classes are characterized as follows.

Pair creation The hard subprocess is one of the two LO parton fusion processes $\mathrm{gg} \to \mathrm{Q}\overline{\mathrm{Q}}$ or $\mathrm{q}\overline{\mathrm{q}} \to \mathrm{Q}\overline{\mathrm{Q}}$. Parton showers do not modify the production cross sections, but only shift kinematics. For instance, in the LO description, the Q and $\overline{\mathrm{Q}}$ have to emerge back-to-back in azimuth in order to conserve momentum, while the parton shower allows a net recoil to be taken by one or several further partons.

Flavour excitation A heavy flavour from the parton distribution of one beam particle is put on mass shell by scattering against a parton of the other beam, i.e. $\mathrm{Qq} \to \mathrm{Qq}$ or $\mathrm{Qg} \to \mathrm{Qg}$. When the Q is not a valence flavour, it must come from a branching $\mathrm{g} \to \mathrm{Q}\overline{\mathrm{Q}}$ of the parton-distribution evolution. In most current sets of parton-distribution functions, heavy-flavour distributions are assumed to vanish for virtuality scales $Q^2 < m_{\mathrm{Q}}^2$. The hard scattering must therefore have a virtuality above m_{Q}^2. When the initial-state shower is reconstructed backwards [9], the $\mathrm{g} \to \mathrm{Q}\overline{\mathrm{Q}}$ branching will be encountered, provided that Q_0, the lower cutoff of the shower, obeys $Q_0^2 < m_{\mathrm{Q}}^2$. Effectively the processes therefore become at least $\mathrm{gq} \to \mathrm{Q}\overline{\mathrm{Q}}\mathrm{q}$ or $\mathrm{gg} \to \mathrm{Q}\overline{\mathrm{Q}}\mathrm{g}$, with the possibility of further emissions. In principle, such final states could also be obtained in the above pair-creation case, but the requirement that the hard scattering must be more virtual than the showers avoids double counting.

Gluon splitting A $\mathrm{g} \to \mathrm{Q}\overline{\mathrm{Q}}$ branching occurs in the initial- or final-state shower but no heavy flavours are produced in the hard scattering. Here the dominant $\mathrm{Q}\overline{\mathrm{Q}}$ source is gluons in the final-state showers since time-like gluons emitted in the initial state are restricted to a smaller maximum virtuality. Except at high energies, most initial state gluon splittings instead result in flavour excitation, already covered above. An ambiguity of terminology exists with initial-state evolution chains where a gluon first branches to $\mathrm{Q}\overline{\mathrm{Q}}$ and the Q later emits another gluon that enters the hard scattering. From an ideological point of view, this is flavour excitation, since it is related to the evolution of the heavy-flavour parton distribution. From a practical point of view, however, we choose to classify it as gluon splitting, since the hard scattering does not contain any heavy flavours.

In summary, the three classes above are then characterized by having 2, 1 or 0, respectively, heavy flavours in the final state of the LO hard subprocess. Another way to proceed is to add next-to-leading order (NLO) perturbative processes, i.e the $\mathcal{O}(\alpha_{\mathrm{s}}^3)$ corrections to the parton fusion [10, 11]. However, with our currently available set of calculational tools, the NLO approach is not so well suited for exclusive Monte Carlo studies where hadronization is added to the partonic picture.

Flavour excitation and gluon splitting give significant contributions to the total b cross section at LHC energies and thus must be considered when this is of interest, see the following. However, NLO calculations probably do a better job on the total b cross section itself (while, for the lighter c quark, production in parton showers is so large that the NLO cross sections are more questionable). The shapes of single heavy quark spectra

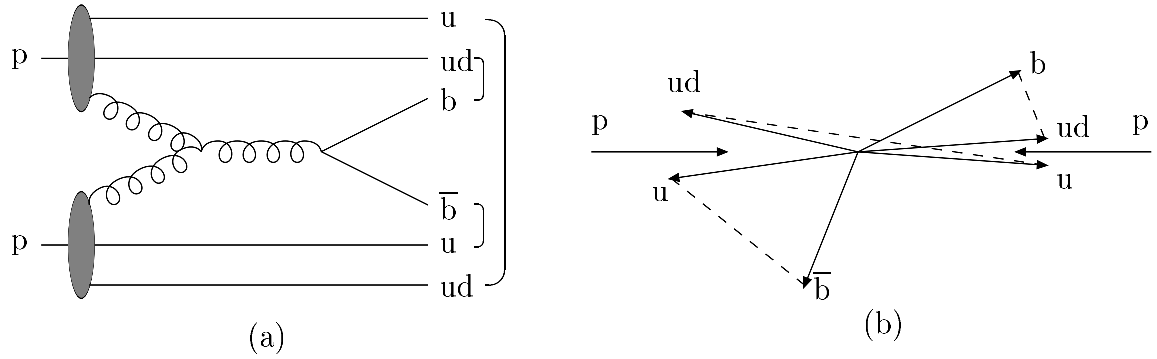

Figure 1: Example of a string configuration in a pp collision. (a) Graph of the process, with brackets denoting the final colour singlet subsystems. (b) Corresponding momentum space picture, with dashed lines denoting the strings.

are not altered as much as the correlations between Q and $\overline{Q}$ when extra production channels are added. Similar observations have been made when comparing NLO to LO calculations [12]. Likewise, asymmetries between single heavy quarks are also not changed much by adding further production channels, so for simplicity we consider only the pair creation process here.

After an event has been generated at the parton level we add fragmentation to obtain a hadronic final state. We use the Lund string fragmentation model. Its effects on charm production were described in [3]. Here we only summarize the main points.

In the string model, confinement is implemented by spanning strings between the outgoing partons. These strings correspond to a Lorentz-invariant description of a linear confinement potential with string tension $\kappa \approx 1$ GeV/fm. Each string piece has a colour charge at one end and its anticolour at the other. The double colour charge of the gluon corresponds to it being attached to two string pieces, while a quark is only attached to one. A diquark is considered as being in a colour antitriplet representation, and thus behaves (in this respect) like an antiquark. Then each string contains a colour triplet endpoint, a number (possibly zero) of intermediate gluons and a colour antitriplet end. An event will normally contain several separate strings, especially at high energies where $g \to q\overline{q}$ splittings occur frequently in the parton shower.

The string topology can be derived from the colour flow of the hard process with some ambiguity arising from colour-suppressed terms. Consider e.g. the LO process $gg \to b\overline{b}$ where two distinct colour topologies are possible. Representing the proton remnant by a u quark and a ud diquark (alternatively d plus uu), one possibility is to have the three strings b–ud, $\overline{b}$–u and u–ud, Fig. 1, and the other is identical except the b is instead connected to the ud diquark of the other proton because the initial state is symmetric.

Once the string topology has been determined, the Lund string fragmentation model [5] can be applied to describe the nonperturbative hadronization. To first approximation, we assume that the hadronization of each colour singlet subsystem, i.e. string, can be considered separately from that of all the other subsystems. Presupposing that the fragmentation mechanism is universal, i.e. process-independent, the good description of e^+e^- annihilation data should carry over. The main difference between e^+e^- and hadron–hadron events is that the latter contain beam remnants which are colour-connected with the hard-scattering partons.

Depending on the invariant mass of a string, practical considerations lead us to distinguish the following three hadronization prescriptions:

Normal string fragmentation In the ideal situation, each string has a large invariant mass. Then the standard iterative fragmentation scheme, for which the assumption of a continuum of phase-space states is essential, works well. The average multiplicity of hadrons produced from a string increases linearly with the string 'length', which means logarithmically with the string mass. In practice, this approach can be used for all strings above some cutoff mass of a few GeV.

Cluster decay If a string is produced with a small invariant mass, perhaps only a single two-body final state is kinematically accessible. In this case the standard iterative Lund scheme is not applicable. We call such a low-mass string a cluster and consider its decay separately. When kinematically possible, a Q–$\overline{\mathrm{q}}$ cluster will decay into one heavy and one light hadron by the production of a light $\mathrm{q}\overline{\mathrm{q}}$ pair in the colour force field between the two cluster endpoints with the new quark flavour selected according to the same rules as in normal string fragmentation. The $\overline{\mathrm{q}}$ cluster end or the new $\mathrm{q}\overline{\mathrm{q}}$ pair may also denote a diquark. In the latest version of PYTHIA, anisotropic decay of a cluster has been introduced, where the mass dependence of the anisotropy has been matched to string fragmentation.

Cluster collapse This is the extreme case of cluster decay, where the string mass is so small that the cluster cannot decay into two hadrons. It is then assumed to collapse directly into a single hadron which inherits the flavour contents of the string endpoints. The original continuum of string/cluster masses is replaced by a discrete set of hadron masses, mainly B and B^* (or the corresponding baryon states). This mechanism plays a special rôle since it allows flavour asymmetries favouring hadron species that can inherit some of the beam-remnant flavour contents. Energy and momentum is not conserved in the collapse so that some energy-momentum has to be taken from, or transferred to, the rest of the event. In the new version, a scheme has been introduced where energy and momentum are shuffled locally in an event.

We assume that the nonperturbative hadronization process does not change the perturbatively calculated total rate of bottom production. By local duality arguments [13], we further presume that the rate of cluster collapse can be obtained from the calculated rate of low-mass strings. In the process $\mathrm{e}^+\mathrm{e}^- \to \mathrm{c}\overline{\mathrm{c}}$ local duality suggests that the sum of the J/ψ and ψ' cross sections approximately equal the perturbative $\mathrm{c}\overline{\mathrm{c}}$ production cross section in the mass interval below the $\mathrm{D}\overline{\mathrm{D}}$-threshold. Similar arguments have also been proposed for τ decay to hadrons [14] and shown to be accurate. In the current case, the presence of other strings in the event also allows soft-gluon exchanges to modify parton momenta as required to obtain the correct hadron masses. Traditional factorization of short- and long-distance physics would then also preserve the total bottom cross section. Local duality and factorization, however, do not specify *how* to conserve the overall energy and momentum of an event when a continuum of $\overline{\mathrm{b}}\mathrm{d}$ masses is to be replaced by a discrete B^0. In practice, however, the different possible hadronization mechanisms do not affect asymmetries much. The fraction of the string-mass distribution below the two particle threshold effectively determines the total rate of cluster collapse and therefore the asymmetry.

The cluster collapse rate depends on several model parameters. The most important ones are listed here with the PYTHIA parameter values that we have used. The PYTHIA parameters are included in the new default parameter set in PYTHIA `6.135` and later versions.

- **Quark masses** The quark masses affect the threshold of the string-mass distribution. Changing the quark mass shifts the string-mass threshold relative to the fixed mass of the lightest two-body hadronic final state of the cluster. Smaller quark masses imply larger below-threshold production and an increased asymmetry. The new default masses are `PMAS(1)`$= m_{\mathrm{u}} =$ `PMAS(2)`$= m_{\mathrm{d}} =$ `0.33D0`, `PMAS(3)`$= m_{\mathrm{s}} =$ `0.5D0`, `PMAS(4)`$= m_{\mathrm{c}} =$ `1.5D0` and `PMAS(5)`$= m_{\mathrm{b}} =$ `4.8D0`.

- **Width of the primordial $k_\perp$ distribution.** If the incoming partons are given small $p_\perp$ kicks in the initial state, asymmetries can appear at larger $p_\perp$ since the beam remnants are given compensating $p_\perp$ kicks, thus allowing collapses at larger $p_\perp$. The new parameters are `PARP(91)=1.D0` and `PARP(93)=5.D0`.

- **Beam remnant distribution functions (BRDF).** When a gluon is picked out of the proton, the rest of the proton forms a beam remnant consisting, to first approximation, of a quark and a diquark. How the remaining energy and momentum should be split between these two is not known from first principles. We therefore use different parameterizations of the splitting function and check the resulting variations. We find significant differences only at large rapidities where an uneven energy-momentum splitting tend to shift bottom quarks connected to a beam remnant diquark more in the direction of the beam remnant, hence giving rise to asymmetries at very large rapidities. We use an intermediate scenario in this study, given by `MSTP(92)=3`.

- **Threshold behaviour between cluster decay and collapse.** Consider a $\mathrm{b\overline{d}}$ cluster with an invariant mass at, or slightly above, the two particle threshold. Should this cluster decay to two hadrons or collapse into one? In one extreme point of view, a $\mathrm{B}\pi$ pair should always be formed when above this threshold, and never a single B. In another extreme, the two-body fraction would gradually increase at a succession of thresholds: $\mathrm{B}\pi$, $\mathrm{B}^*\pi$, $\mathrm{B}\rho$, $\mathrm{B}^*\rho$, etc., where the relative probability for each channel is given by the standard flavour and spin mixture in string fragmentation. In our current default model, we have chosen to steer a middle course by allowing two attempts (`MSTJ(17)=2`) to find a possible pair of hadrons. Thus a fraction of events may collapse to a single resonance also above the $\mathrm{B}\pi$ threshold, but $\mathrm{B}\pi$ is effectively weighted up. If a large number of attempts had been allowed (this can be varied using the free parameter `MSTJ(17)`), collapse would only become possible for cluster masses below the $\mathrm{B}\pi$ threshold.

The colour connection between the produced heavy quarks and the beam remnants in the string model gives rise to an effect called beam remnant drag. In an independent fragmentation scenario the light cone energy momentum of the quark is simply scaled by some factor picked from a fragmentation function. Thus, on average the rapidity is conserved in the fragmentation process. This is not necessarily so in string fragmentation, where both string ends contribute to the four-momentum of the produced heavy hadron. If the other end of the string is a beam remnant, the hadron will be shifted in rapidity in the direction of the beam remnant resulting in an increase in $|y|$. This beam-drag is

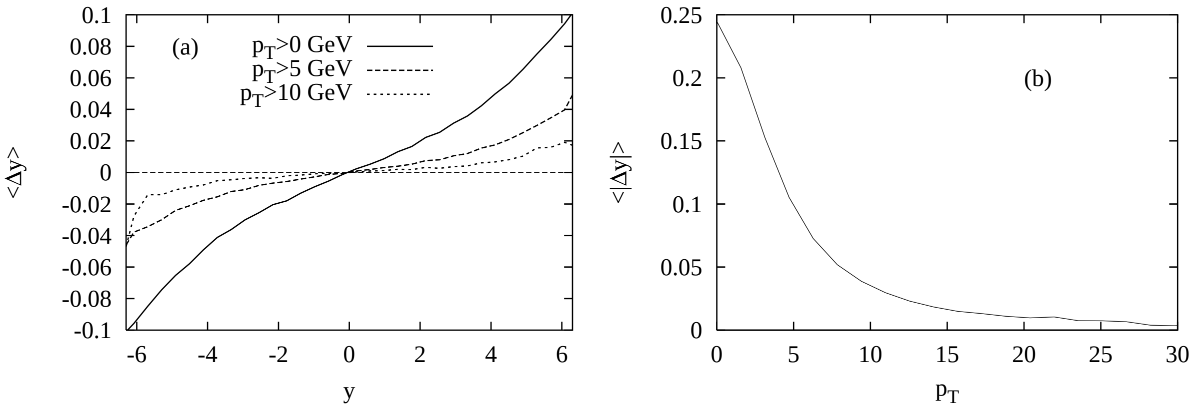

Figure 2: (a) Average rapidity shift $\Delta y = \langle y_{\rm B} - y_{\rm b}\rangle$ as a function of y for some different $p_\perp$ cuts. (b) Average rapidity shift $\langle|\Delta y|\rangle$ in the direction of "the other end of the string" that the bottom quark is connected to, i.e. ignoring the sign of the shift.

shown qualitatively in Fig. 2, where the rapidity shift is shown as a function of rapidity and transverse momentum. This shift is not directly accessible experimentally, only indirectly as a discrepancy between the shape of perturbatively calculated quark distributions and the data.

3 Intrinsic Heavy Quarks

The wavefunction of a hadron in QCD can be represented as a superposition of Fock state fluctuations, e.g. $|n_{\rm V}\rangle$, $|n_{\rm V}{\rm g}\rangle$, $|n_{\rm V}{\rm Q}\overline{\rm Q}\rangle$, ... components where $n_{\rm V} \equiv$ uud for a proton. When the projectile scatters in the target, the coherence of the Fock components is broken and the fluctuations can hadronize either by uncorrelated fragmentation as for leading twist production or coalescence with spectator quarks in the wavefunction [4, 7]. The intrinsic heavy quark Fock components are generated by virtual interactions such as ${\rm gg} \rightarrow {\rm Q}\overline{\rm Q}$ where the gluons couple to two or more projectile valence quarks. Intrinsic ${\rm Q}\overline{\rm Q}$ Fock states are dominated by configurations with equal rapidity constituents so that, unlike sea quarks generated from a single parton, the intrinsic heavy quarks carry a large fraction of the parent momentum [4].

The frame-independent probability distribution of an n–particle ${\rm b}\overline{\rm b}$ Fock state is

$$\frac{dP^n_{\rm ib}}{dx_i \cdots dx_n} = N_n \frac{\delta(1 - \sum_{i=1}^n x_i)}{(m_h^2 - \sum_{i=1}^n (\widehat{m}_i^2/x_i))^2} \ , \tag{1}$$

where $\widehat{m}_i^2 = k_{\perp,i}^2 + m_i^2$ is the effective transverse mass of the $i^{\rm th}$ particle and x_i is the light-cone momentum fraction. The probability, $P^n_{\rm ib}$, is normalized by N_n and $n = 5$ for baryon production from the $|n_{\rm V}{\rm b}\overline{\rm b}\rangle$ configuration. The delta function conserves longitudinal momentum. The dominant Fock configurations are closest to the light-cone energy shell and therefore the invariant mass, $M^2 = \sum_i \widehat{m}_i^2/x_i$, is minimized. Assuming $\langle \vec{k}_{\perp,i}^2\rangle$ is proportional to the square of the constituent quark mass, we choose $\widehat{m}_{\rm q} = 0.45$ GeV, $\widehat{m}_{\rm s} = 0.71$ GeV, and $\widehat{m}_{\rm b} = 5$ GeV [15, 16].

The $x_{\rm F}$ distribution for a single bottom hadron produced from an n-particle intrinsic bottom state can be related to $P^n_{\rm ib}$ and the inelastic pp cross section by

$$\frac{\sigma^H_{\rm ib}({\rm pp})}{dx_{\rm F}} = \frac{dP_H}{dx_{\rm F}} \sigma^{\rm in}_{\rm pp} \frac{\mu^2}{4\widehat{m}^2_{\rm b}} \alpha^4_s(M_{\rm b\overline{b}}) \ . \tag{2}$$

The probability distribution is the sum of all contributions from the $|n_{\rm V}{\rm b\overline{b}}\rangle$ and the $|n_{\rm V}{\rm b\overline{b}q\overline{q}}\rangle$ configurations with q = u, d, and s and includes uncorrelated fragmentation and coalescence, as described below, when appropriate [17]. The factor of $\mu^2/4\widehat{m}^2_{\rm b}$ arises from the soft interaction which breaks the coherence of the Fock state. We take $\mu^2 \sim 0.1$ GeV^2 [18]. The intrinsic charm probability, $P^5_{\rm ic} = 0.31\%$, was determined from analyses of the EMC charm structure function data [19]. The intrinsic bottom probability is scaled from the intrinsic charm probability by the square of the transverse masses, $P_{\rm ib} = P_{\rm ic}(\widehat{m}_{\rm c}/\widehat{m}_{\rm b})^2$. The intrinsic bottom cross section is reduced relative to the intrinsic charm cross section by a factor of $\alpha^4_{\rm s}(M_{\rm b\overline{b}})/\alpha^4_{\rm s}(M_{\rm c\overline{c}})$ [20]. Taking these factors into account, we obtain $\sigma^5_{\rm ib}(pN) \approx 7$ nb at 14 TeV.

There are two ways of producing bottom hadrons from intrinsic ${\rm b\overline{b}}$ states. The first is by uncorrelated fragmentation. If we assume that the b quark fragments into a B meson, the B distribution is

$$\frac{dP^{nF}_{\rm ib}}{dx_{\rm B}} = \int dz \prod_{i=1}^n dx_i \frac{dP^n_{\rm ib}}{dx_1 \ldots dx_n} \frac{D_{B/b}(z)}{z} \delta(x_{\rm B} - zx_{\rm b}) \ , \tag{3}$$

These distributions are assumed for all intrinsic bottom production by uncorrelated fragmentation with $D_{H/b}(z) = \delta(z-1)$. At low $p_\perp$, this approximation should not be too bad, as seen in fixed target production [16].

If the projectile has the corresponding valence quarks, the bottom quark can also hadronize by coalescence with the valence spectators. The coalescence distributions are specific for the individual bottom hadrons. It is reasonable to assume that the intrinsic bottom Fock states are fragile and can easily materialize into bottom hadrons in high-energy, low momentum transfer reactions through coalescence. The coalescence contribution to bottom hadron production is

$$\frac{dP^{nC}_{\rm ib}}{dx_H} = \int \prod_{i=1}^n dx_i \frac{dP^n_{\rm ib}}{dx_1 \ldots dx_n} \delta(x_H - x_{H_1} - \cdots - x_{H_{n_{\rm V}}}) \ . \tag{4}$$

where the coalescence function is simply a delta function combining the momentum fractions of the quarks in the Fock state configuration that make up the valence quarks of the final-state hadron.

Not all bottom hadrons can be produced from the minimal intrinsic bottom Fock state configuration, $|n_{\rm V}{\rm b\overline{b}}\rangle$. However, coalescence can also occur within higher fluctuations of the intrinsic bottom Fock state. For example, in the proton, the ${\rm B}^-$ and $\Xi^0_{\rm b}$ can be produced by coalescence from $|n_{\rm V}{\rm b\overline{b}u\overline{u}}\rangle$ and $|n_{\rm V}{\rm b\overline{b}s\overline{s}}\rangle$ configurations. These higher Fock state probabilities can be obtained using earlier results on $\psi\psi$ pair production [21, 22]. If all the measured $\psi\psi$ pairs [23] arise from $|n_{\rm V}{\rm c\overline{c}c\overline{c}}\rangle$ configurations, $P_{\rm icc} \approx 4.4\%\ P_{\rm ic}$ [22, 24]. It was found that the probability of a $|n_{\rm V}{\rm c\overline{c}q\overline{q}}\rangle$ state was then $P_{\rm icq} = (\hat{m}_{\rm c}/\hat{m}_{\rm q})^2 P_{\rm icc}$ [21]. If we then assume $P_{\rm ibq} = (\hat{m}_{\rm c}/\hat{m}_{\rm b})^2 P_{\rm icq}$, we find that

$$P_{\rm ibq} \approx \left(\frac{\widehat{m}_{\rm c}}{\widehat{m}_{\rm b}}\right)^2 \left(\frac{\widehat{m}_{\rm c}}{\widehat{m}_{\rm q}}\right)^2 P_{\rm icc} \ , \tag{5}$$

leading to $P_{\rm ibu} = P_{\rm ibd} \approx 70.4\%\ P_{\rm ib}$ and $P_{\rm ibs} \approx 28.5\%\ P_{\rm ib}$. To go to still higher configurations, one can make similar assumptions. However, as more partons are included

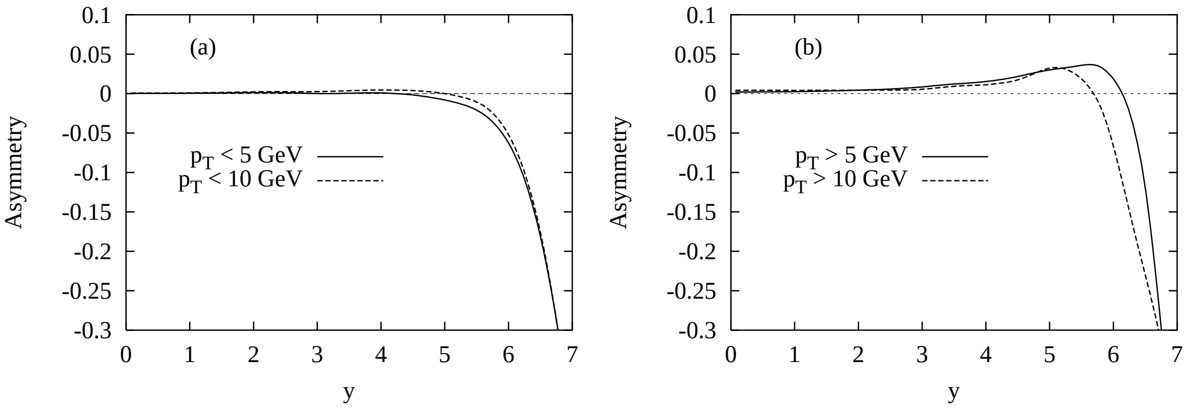

Figure 3: The asymmetry, $A = \frac{\sigma(\mathrm{B}^0)-\sigma(\overline{\mathrm{B}}^0)}{\sigma(\mathrm{B}^0)+\sigma(\overline{\mathrm{B}}^0)}$, as a function of rapidity for different $p_\perp$ cuts: (a) $p_\perp < 5, 10$ GeV and (b) $p_\perp > 5, 10$ GeV using parameter set 1 as described in the text.

in the Fock state, the coalescence distributions soften and approach the fragmentation distributions, eventually producing bottom hadrons with less momentum than uncorrelated fragmentation from the minimal $\mathrm{b\overline{b}}$ state if a sufficient number of $\mathrm{q\overline{q}}$ pairs are included. There is then no longer any advantage to introducing more light quark pairs into the configuration—the relative probability will decrease while the potential gain in momentum is not significant. Therefore, we consider production by fragmentation and coalescence from the minimal state and the next higher states with $\mathrm{u\overline{u}}$, $\mathrm{d\overline{d}}$ and $\mathrm{s\overline{s}}$ pairs.

The probability distributions entering Eq. (2) for B^0 and $\overline{\mathrm{B}}^0$ are

$$\begin{aligned} \frac{dP_{\mathrm{B}^0}}{dx_{\mathrm{F}}} &= \frac{1}{2}\left(\frac{1}{10}\frac{dP^{5F}_{\mathrm{ib}}}{dx_{\mathrm{F}}} + \frac{1}{4}\frac{dP^{5C}_{\mathrm{ib}}}{dx_{\mathrm{F}}}\right) + \frac{1}{2}\left(\frac{1}{10}\frac{dP^{7F}_{\mathrm{ibu}}}{dx_{\mathrm{F}}} + \frac{1}{5}\frac{dP^{7C}_{\mathrm{ibu}}}{dx_{\mathrm{F}}}\right) \\ &\quad + \frac{1}{2}\left(\frac{1}{10}\frac{dP^{7F}_{\mathrm{ibd}}}{dx_{\mathrm{F}}} + \frac{2}{5}\frac{dP^{7C}_{\mathrm{ibd}}}{dx_{\mathrm{F}}}\right) + \frac{1}{2}\left(\frac{1}{10}\frac{dP^{7F}_{\mathrm{ibs}}}{dx_{\mathrm{F}}} + \frac{1}{5}\frac{dP^{7C}_{\mathrm{ibs}}}{dx_{\mathrm{F}}}\right) \qquad (6) \\ \frac{dP_{\overline{\mathrm{B}}^0}}{dx_{\mathrm{F}}} &= \frac{1}{10}\frac{dP^{5F}_{\mathrm{ib}}}{dx_{\mathrm{F}}} + \frac{1}{10}\frac{dP^{7F}_{\mathrm{ibu}}}{dx_{\mathrm{F}}} + \frac{1}{2}\left(\frac{1}{10}\frac{dP^{7F}_{\mathrm{ibd}}}{dx_{\mathrm{F}}} + \frac{1}{8}\frac{dP^{7C}_{\mathrm{ibd}}}{dx_{\mathrm{F}}}\right) + \frac{1}{10}\frac{dP^{7F}_{\mathrm{ibs}}}{dx_{\mathrm{F}}}\ . \qquad (7) \end{aligned}$$

See Ref. [17] for more details and the probability distributions of other bottom hadrons.

4 Model predictions

In this section we present some results from both models. Fig. 3 shows the asymmetry between B^0 and $\overline{\mathrm{B}}^0$ as a function of y for several $p_\perp$ cuts in the string model. The asymmetry is essentially zero for central rapidities and increases slowly with rapidity. When the kinematical limit is approached, the asymmetry changes sign for small $p_\perp$ because of the drag-effect since b-quarks are often connected to diquarks from the proton beam remnant, Fig. 1, thus producing $\overline{\mathrm{B}}^0$ hadrons which are shifted more in rapidity than B^0. Cluster collapse, on the other hand, tend to enhance the production of leading particles (in this case B^0) so the two mechanisms give rise to asymmetries with different signs. Collapse is the main effect at small rapidities while eventually at very large y, the drag effect dominates.

Parameters	$\|y\| < 2.5$, $p_\perp > 5$ GeV	$3 < \|y\| < 5$, $p_\perp > 5$ GeV	$\|y\| > 3$, $p_\perp < 5$ GeV
Set 1	0.003(1)	0.015(2)	−0.008(1)
Set 2	−0.000(2)	0.009(3)	−0.005(2)
Set 3	0.013(2)	0.020(3)	−0.018(2)

Table 1: Parameter dependence of the asymmetry in the string model. The statistical error in the last digit is shown in parenthesis (95% confidence).

In Table 1 we study the parameter dependence of the asymmetry by looking at the integrated asymmetry for different kinematical regions using three different parameter sets:

- **Set 1** is the new default as presented in Section 2.
- **Set 2** The same as Set 1 except it uses simple counting rules in the beam remnant splitting, i.e. each quark get on average one third of the beam remnant energy-momentum.
- **Set 3** The old parameter set, before fitting to fixed-target data, is included as a reference. This set is characterized by current algebra masses, lower intrinsic $k_\perp$, and an uneven sharing of beam remnant energy-momentum.

We see that in the central region the asymmetry is generally very small whereas for forward (but not extremely forward) rapidities and moderate $p_\perp$ the asymmetry is around 1–2%. In the very forward region at small $p_\perp$, drag asymmetry dominates which can be seen from the change in sign of the asymmetry. The asymmetry is fairly stable under moderate variations in the parameters even though the difference between the old and new parameter sets (Set 1 and 3) are large in the central region. Set 1 typically gives rise to smaller asymmetries.

The cross sections for all intrinsic bottom hadrons are given as a function of x_F in Fig. 4. The bottom baryon distributions are shown in Fig. 4(a). The Λ_b^0 (Σ_b^0) distributions are the largest and most forward peaked of all the distributions. The Σ_b^- is the smallest and the softest, similar to that of the bottom-strange mesons and baryons shown in Fig. 4(b). The different coalescence probabilities assumed for hadrons from the $|\mathrm{uudb\overline{b}s\overline{s}}\rangle$ configuration have little real effect on the shape of the cross section, dominated by independent fragmentation. Of the B mesons shown in Fig. 4(c), the B^+ and B^0 cross sections are the largest since both can be produced from the 5 particle configuration. The B^- and $\overline{\mathrm{B}}^0$ distributions are virtually identical. We note that the x_F distributions of other bottom hadrons not included in the figure would be similar to the bottom-strange hadrons since they would be produced by fragmentation only.

The x_F distribution for final-state hadron H is the sum of the leading-twist fusion and intrinsic bottom components,

$$\frac{d\sigma_{hN}^H}{dx_\mathrm{F}} = \frac{d\sigma_\mathrm{lt}^H}{dx_\mathrm{F}} + \frac{d\sigma_\mathrm{ib}^H}{dx_\mathrm{F}} \; . \tag{8}$$

The intrinsic bottom cross sections from Section 3 are combined with a leading twist calculation using independent fragmentation where drag effects are not included. The leading twist results have been smoothed and extrapolated to large x_F to facilitate a

[3] Thanks to J. Klay at UC Davis for extending the curves to large x_F.

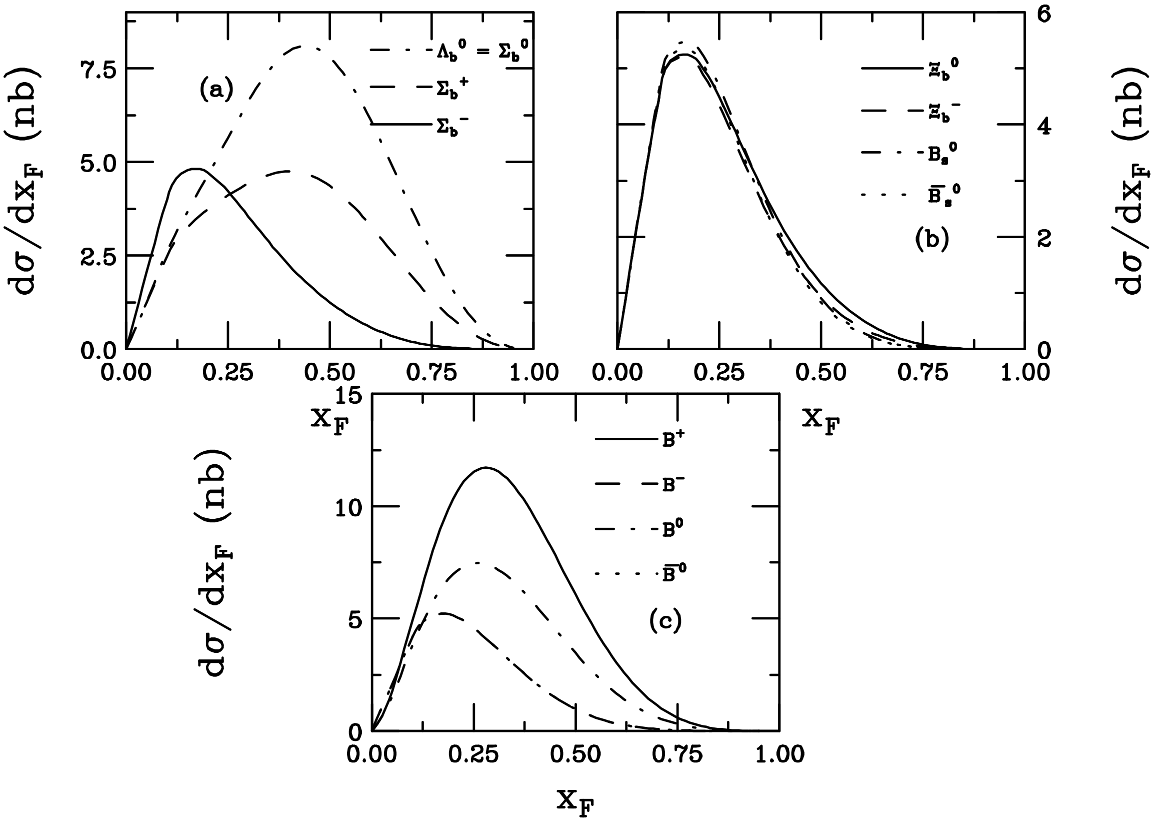

Figure 4: Predictions for bottom hadron production are given for pp collisions at 14 TeV. The bottom baryon distributions are given in (a) for $\Lambda_{\rm b}^0 = \Sigma_{\rm b}^0$ (dot-dashed), $\Sigma_{\rm b}^+$ (dashed), and $\Sigma_{\rm b}^-$ (solid). The bottom-strange distributions are shown in (b) for $\Xi_{\rm b}^0$ (solid), $\Xi_{\rm b}^-$ (dashed), $\rm B_s^0$ (dot-dashed), and $\overline{\rm B}_s^0$ (dotted). In (c), the B meson distributions are given: $\rm B^+$ (solid), $\rm B^-$ (dashed), $\rm B^0$ (dot-dashed), and $\overline{\rm B}^0$ (dotted). The $\rm B^-$ and $\overline{\rm B}^0$ distributions are virtually identical.

comparison with the intrinsic bottom calculation. The resulting total $\rm B^0$ and $\overline{\rm B}^0$ distributions are shown in Fig. 5, along with the corresponding asymmetry. Note that since the intrinsic heavy quark $p_\perp$ distributions are more steeply falling than the leading twist, we only consider $p_\perp < 5$ GeV. The distributions are drawn to emphasize the high $x_{\rm F}$ region where the distributions differ. The asymmetry is ~ 0.1 at $x_{\rm F} \sim 0.25$, corresponding to $y \sim 6.5$. Therefore, intrinsic bottom should not be a significant source of asymmetries.

5 Summary

To summarize, we have studied possible production asymmetries between b and $\overline{\rm b}$ hadrons, especially $\rm B^0$ and $\overline{\rm B}^0$, as predicted by the Lund string fragmentation model and the intrinsic heavy quark model. We find negligible asymmetries for central rapidities and large $p_\perp$ (in general, less than 1%). For some especially favoured kinematical ranges such as $y > 3$ and $5 < p_\perp < 10$ GeV the collapse asymmetry could be as high as 1–2%. Intrinsic bottom becomes important only for $x_{\rm F} > 0.25$ and $p_\perp < 5$ GeV, corresponding to $y > 6.5$.

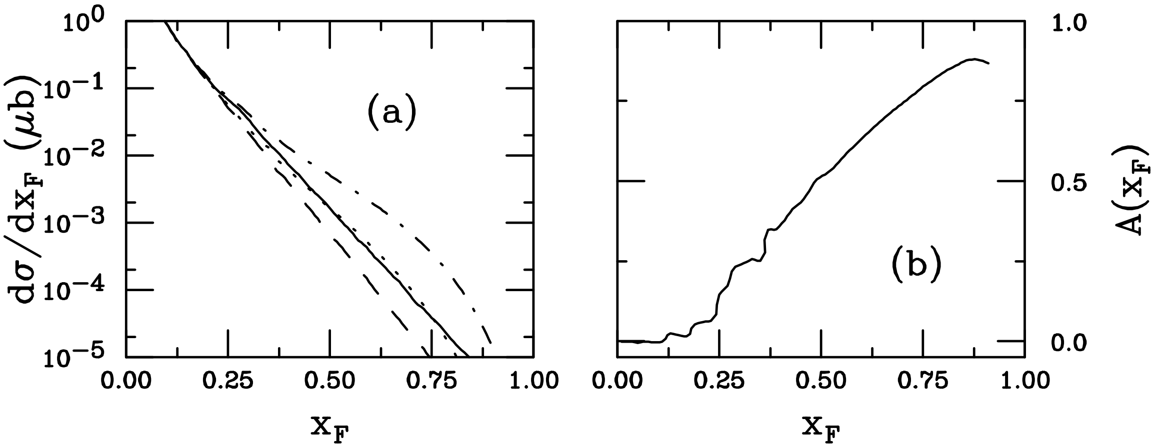

Figure 5: (a) Leading-twist predictions for B^0 (solid) and $\overline{B}^0$ (dashed) using independent fragmentation. Model predictions for B^0 (dot-dashed) and $\overline{B}^0$ (dotted) distributions from Eq. (8). (b) The asymmetry between B^0 and $\overline{B}^0$, the dot-dashed and dotted curves in (a), is also given.

References

[1] WA82 Collaboration, M. Adamovich et al., Phys. Lett. **B305** (1993) 402; E769 Collaboration, G.A. Alves et al., Phys. Rev. Lett. **72** (1994) 812; E791 Collaboration, E.M. Aitala et al., Phys. Lett. **B371** (1996) 157.

[2] E. Norrbin, proceedings of the International Europhysics Conference on High-Energy Physics (EPS-HEP 99), Tampere, Finland, 15-21 July 1999, LU-TP-99-28, hep-ph/9909437.

[3] E. Norrbin and T. Sjöstrand, Phys. Lett. **B442** (1998) 407, in preparation.

[4] S.J. Brodsky, P. Hoyer, C. Peterson and N. Sakai, Phys. Lett. **B93** (1980) 451; S.J. Brodsky, C. Peterson and N. Sakai, Phys. Rev. **D23** (1981) 2745.

[5] B. Andersson, G. Gustafson, G. Ingelman and T. Sjöstrand, Phys. Rep. **97** (1983) 31.

[6] R. Vogt and S.J. Brodsky, Nucl. Phys. **B438** (1995) 261.

[7] S.J. Brodsky, P. Hoyer, A.H. Mueller and W.-K. Tang, Nucl. Phys. **B369** (1992) 519.

[8] T. Sjöstrand, Comput. Phys. Commun. **82** (1994) 74.

[9] T. Sjöstrand, Phys. Lett. **B157** (1985) 321.

[10] P. Nason, S. Dawson and R. K. Ellis, Nucl. Phys. **B327**, 49 (1989); erratum ibid. **B335**, 260 (1990).

[11] W. Beenakker, W.L. van Neerven, R. Meng, G.A. Schuler and J. Smith, Nucl. Phys. **B351**, 507 (1991).

[12] M.L. Mangano, P. Nason and G. Ridolfi, Nucl. Phys. **B405** (1993) 507

[13] E.D. Bloom and F.J. Gilman, Phys. Rev. **D4** (1971) 2901; J.J. Sakurai, Phys. Lett. **46B** (1973) 207; H. Fritzsch, Phys. Lett. **67B** (1977) 217; R.A. Bertlmann, G. Launer and E. de Rafael, Nucl. Phys. **B250** (1985) 61; and references therein.

[14] E. Braaten, S. Narison and A. Pich, Nucl. Phys. **B373** (1992) 581.

[15] R. Vogt, S.J. Brodsky and P. Hoyer, Nucl. Phys. **B360** (1991) 67.

[16] R. Vogt, S.J. Brodsky and P. Hoyer, Nucl. Phys. **B383** (1992) 643.

[17] R. Vogt, LBNL-43095, in the proceedings of the LHC Working Group on b Production, P. Nason and G. Ridolfi covenors, CERN, 4/99. The proceedings are available on the web at http://home.cern.ch/n/nason/www/lhc99/15-04-99/.

[18] T. Gutierrez and R. Vogt, Nucl. Phys. **B539** (1999) 189.

[19] J.J. Aubert et al. (EMC Collab.), Phys. Lett. **110B** (1982) 73; E. Hoffmann and R. Moore, Z. Phys. **C20** (1983) 71; B.W. Harris, J. Smith, and R. Vogt, Nucl. Phys. **B461** (1996) 181.

[20] R. Vogt and S.J. Brodsky, Nucl. Phys. **B438** (1995) 261.

[21] R. Vogt and S.J. Brodsky, Nucl. Phys. **B478** (1996) 311.

[22] R. Vogt and S.J. Brodsky, Phys. Lett. **B349** (1995) 569.

[23] J. Badier et al. (NA3 Collab.), Phys. Lett. **114B** (1982) 457; **158B** (1985) 85.

[24] R. Vogt, Nucl. Phys. **B446**, (1995) 159.